Supporting Information

Ion-directed polymer/inorganic interphase with enriched charge for the stable and high-rate Zn anode

Meihua Zhu[a], Sitian Ku[b], Qing Ran[c], Houhou Huang[b], Ningzhi Cao[a], Fu-Quan Bai*[b], Xing-You Lang*[c], Danming Chao*[a] and Ming Feng*[d]

a M. Zhu, N. Cao and D. Chao

National and Local Joint Engineering Laboratory for Synthetic Technology of High Performance Polymer, College of Chemistry, Jilin University, Changchun, 130012, China

Email: chaodanming@jlu.edu.cn

b S. Ku, H. Huang, F.-Q. Bai

International Joint Research Laboratory of Nano-Micro Architecture Chemistry, Institute of Theoretical Chemistry and College of Chemistry, Jilin University, Changchun, 130021, China

Email: baifq@jlu.edu.cn

c Q. Ran, X.-Y. Lang

Key Laboratory of Automobile Materials, Ministry of Education, School of Materials Science and Engineering, Jilin University, Changchun 130022, China

Email: xylang@jlu.edu.cn

d M. Feng

Key Laboratory of Functional Materials Physics and Chemistry of the Ministry of Education, Jilin Normal University, Changchun, 130103, China

Email: mingfeng@jlnu.edu.cn

Experimental Section

Materials

Commercial Ti foil (10 μm), Cu foil (10 μm), stainless mesh (250 mesh), and Zn foil (100 and 20 μm) were purchased from Saibo of Beijing. All the chemical reagents were purchased from Aladdin without further purification.

Preparation of Polymer-Zn (PZn) Anode

Firstly, the EDOT-SO_3Na monomer was synthesized according to our previous work. Then, the water-processed conducting polymer (PEDOT-SO_3H, PEDOT-SH) was prepared by typical chemical oxidization polymerization: The EDOT-SO_3Na monomer (5 g, 15 mmol) and $FeSO_4 \cdot 7H_2O$ (2.52 g, 9 mmol) were dissolved in a 1 M H_2SO_4 solution with continuous stirring. After thorough dissolution, $(NH_4)_2S_2O_8$ (6.89 g, 30.2 mmol) in deionized water was added dropwise to the above solution under an Argon atmosphere. The reaction started with the black solution and was quenched by acetone after one day. The product was then precipitated from acetone, centrifuged (5000 rpm, 5 min), followed by dissolution in water. After repeating 3 times, the black powder (PEDOT-SH) was obtained by dialysis and freeze-drying.

Subsequently, PEDOT-SH was dispersed in water to prepare a water-processed dispersion of 10 mg mL^{-1}. 20 μL of the polymer dispersion was drop-coated onto the polished Zn foil (12 mm diameter), and the PZn anode was finally obtained after drying overnight in a vacuum.

Besides, cross-linked polymer (PEDOT-SO_3Zn) was obtained by adding the PEDOT-SH to an excess 2 M $ZnSO_4$ solution, which replaced the proton with Zn^{2+}. After filtrations, several washings, and drying overnight, neutral polymer, PEDOT-SO_3Zn was collected as black powder. To prepare the polymer-coated Zn electrode without LZHS formation, neutral polymer and PVDF were milled with a mass ratio of 9:1 and then dispersed in N-Methyl pyrrolidone (NMP). The uniform slurry was also coated on the polished Zn foil, and the Zn-P anode was finally obtained after drying at 80°C in a vacuum overnight.

Similarly, the Ti foil and Cu foil were modified with the conducting polymer to obtain a PTi or PCu (Cu-P) electrode.

Preparation of $K_{0.28}MnO_2 \cdot 0.19H_2O$ (KMO) Cathode

Firstly, KMO powder was synthesized by a typical hydrothermal reaction using the sol-gel method: 3 g of $KMnO_4$ was dissolved in 50 mL of H_2O to form solution A, and 5 g of D(+)-glucose was dissolved in 20 mL of H_2O to form solution B. Then, the above solution was mixed quickly and stirred vigorously for 15 s to form a reddish sol, whose color turned brown. After standing and cooling in the air for 30 min, the water was poured out repeatedly and then vacuum dried at 110 °C overnight to obtain the dried gel, followed by calcinating at 400 °C for 2 h. Finally, the brown powder (KMO) was obtained by washing and drying overnight at 60°C.

For the cathode, a self-supported membrane was prepared by mixing KMO powder, acetylene black, and polytetrafluoroethylene (PTFE) in a mass ratio of 7:2:1. The membrane was rolled and compacted onto a stainless steel (SS) mesh, vacuum dried, and finally cut into a special size (1 × 1 cm^2). The average mass loading was 2 mg cm^{-2}. To assemble the pouch cell, the high-loading cathodes were also prepared by mixing KMO, MWCNT, and PTFE (m/m, 7/2/1). The final cathodes were cut into a special size (8 ×8 cm^2) with a loading of 6.6 mg cm^{-2}.

Preparation of Half Cells and Full Cells

All the coin cells were assembled using CR2025 types. The half cells include symmetric batteries and asymmetric batteries. The symmetric battery was assembled by pairing two identical electrodes, such as Zn-Zn (13 mm, 100 μm) as cathode and anode. 120 μL 2 M $ZnSO_4$ aqueous solution and glass fiber filters (GF/C, Whatman) were used as the electrolyte and separator, respectively. The asymmetric batteries were assembled using a Zn anode and Cu (Ti) cathode with the same electrolyte and separators. The full cells were assembled using a KMO cathode and Zn anode, glass fiber (GF/C, Whatman) separator, and 2 M $ZnSO_4$ + 0.2 M $MnSO_4$ electrolytes.

Characterizations

The morphology of Zn anodes before/after deposition was characterized using a field emission scanning electron microscope (SEM, FEI Nova Nano SEM 450) equipped with energy-dispersive spectroscopy (EDS). X-ray diffraction (XRD, D/max-2500PC, Cu Kα radiation) was used to characterize the KMO crystal structure, polymer powder, and Zn anodes before/after Zn deposition. Grazing Incidence Wide-Angle X-ray Scattering (GIWAXS) was performed on the Xeuss3.0 with an incidence angle (0.6°) to investigate the structure of the polymer before/after coating on the Zn metal. X-ray photoelectron spectroscopy (XPS, Thermo ECALAB 250, using Al anodes) was used to study the chemical components of cycled products after Zn deposition with C 1s peak calibration (284.8 eV). Raman spectroscopy was performed on an inVia-Plus 532 spectrometer to obtain the molecular structure of the PZn coating and the electrode/electrolyte interface during cycles. Optical images of the plating Zn were obtained using a self-made in-situ optical-electrochemical cell on an optical microscope (BXFM-ILHS). The gas volume (mainly H_2) was captured and evaluated by a gas chromatography (SHIMADZU GC-2014) with a thermal conductivity detector (TCD), which was blown out of the pouch cell by Ar gas after per 10 cycles. The roughness of the cycled Zn was obtained on the Atomic Force Microscopy (AFM, MFP-3D Infinity, Asylum Research produced by Oxford, UK).

Electrochemical Measurements

The Tafel curves, nucleation overpotentials, and chronoamperometry (CA) curves were tested in 2 M $ZnSO_4$ electrolyte using a three-electrode configuration: Zn (or PZn) as the working electrode, Zn foil as the counter electrode, and Zn wire as the reference electrode. The hydrogen evolution reaction (HER) activity was evaluated in 2 M Na_2SO_4 electrolyte using linear sweep voltammetry (LSV) with the same three-electrode configuration. All three electrode configurations were performed on a CHI660e electrochemical workstation. The electrochemical impedance spectroscopy (EIS) spectra of symmetric and full cells were recorded on the CHI660e, ranging from 10^{-2} to 10^5 Hz. Cyclic voltammetry (CV) curves of the half-cells and full cells were also collected on the CHI660e. The rate performance and cycling stability of the half

cells and full cells were tested using galvanostatic charge-discharge (GCD) tests on the Neware Battery Testing System (CT2001A-5V50mA).

The differential capacitance was evaluated by alternating current (AC) voltammetry using Zn-Cu cells ranging from 0.7 to 0.3 V vs. Zn/Zn^{2+}at a scan rate of 2 mV s^{-1}. The frequency was 6 Hz, and the amplitude was 5 mV. For the in-situ Raman tests, to allow the laser to focus on the electrode/electrolyte interface, the middle area of the glass fiber separator and the Zn anode were punched with a hole (diameter: 2.0 mm). The assembled cell was discharged and charged at 5 mA cm^{-2}/5 mAh cm^{-2}, and the Raman spectra were collected per 3 min with a 532 nm laser during the plating/stripping process. For the in-situ distribution of relaxation time (DRT) analysis, the EIS of Zn-Zn cells was collected at 600 s per time and a total of 12 times per cycle at 1 mA cm^{-2} based on the Galvanostatic Electrochemical Impedance Spectroscopy (GEIS). The frequency ranged from 10^5 to 0.1 Hz.

The pH of the 2 M $ZnSO_4$ electrolyte at the anode/electrolyte interface during the stripping/plating process was monitored using a two-electrode configuration in a 50 mL H-type cell with the same Zn (PZn) as the positive electrode and another Zn (PZn) as the negative electrode.

The ionic transference number was evaluated using a symmetric battery based on Equation 1:

$$t_+ = \frac{I_S(\Delta V - I_0 R_0)}{I_0(\Delta V - I_s R_s)} \quad (1)$$

where ΔV was the polarization voltage (10 mV); I_0 and R_0 were the initial current and resistance, respectively; and I_s and R_s were the steady-state current and resistance.

The exchange current density (i_0) of the electrode was calculated by Equation 2:

$$i = \frac{i_0 \times F \times \eta_{total}}{2 \times R \times T} \quad (2)$$

where i and η were the current density and total overpotentials, respectively. F, R, and T represented the faradic constant (96485 C mol^{-1}), ideal gas constant (8.314 J $mol^{-1}\cdot K^{-1}$), and Kelvin temperature, respectively.

The activation energy (E_a) of the anode in the Zn//Zn cell was calculated according to Equation 3:

$$\frac{1}{R_{ct}} = A \times exp\left(\frac{-E_a}{RT}\right) \quad (3)$$

where R and T stood for the ideal gas constant (8.314 J $mol^{-1}\cdot K^{-1}$) and Kelvin temperature, respectively.

The coulombic efficiency (CE) in the Zn-Cu asymmetric cells was calculated by Equation 4:

$$CE = \frac{Q_s + 9 \times Q_c}{Q_p + 9 \times Q_c} \times 100\% \quad (4)$$

where Q_s and Q_p represented the final stripped capacity/pre-plated capacity in asymmetric batteries. Q_c represented the plating/stripping capacity during cycles.

The cumulative plating capacity (CPC) of the anode was calculated in Zn//Zn cells according to Equation 5:

$$CPC = I_{plating} \times t_{plating} \quad (5)$$

where $I_{plating}$ and $t_{plating}$ represented the discharging current density (mA cm^{-2}) and total discharging time (h), respectively.

Computational simulation

DFT was performed in the Gaussian 16 program with the parameter hybrid method using the Lee–Yang–Parr correlation functional (B3LYP). The basis was set to 6-311+G (d, p), with the GD3BJ dispersion correction, and the solvation effect was considered with the universal solvent (water) of SMD. Before the binding energy calculations, the initial models were optimized, and a frequency calculation was

performed to obtain the optimized geometry structure. The binding energy (E_b) between cations and conducting polymer was calculated based on the following Equation 6:

$$E_b = E_{total} - E_{cations} - E_{polymer} \quad (6)$$

where E_{total}, $E_{cations,}$ and $E_{polymer}$ represented the total energy of complex systems, Zn^{2+} (or H^+) and PEDOT-SO_3^-, respectively.

The selective adsorption process of zinc atoms on the Zn(002) surface and the polymer coating was conducted using semi-empirical ab initio molecular dynamics (SE-AIMD) simulations. In our work, a tetramer polymer unit was placed on a four-layer Zn(002) slab containing 786 zinc atoms, and two additional zinc atoms were randomly positioned above the tetramer unit. Program CP2K (version 2024.3) was used to perform the SE-AIMD calculations, in which the semi-empirical tight binding method called GFN1-xTB was used to perform the single-point energy calculations. The total GFN1-xTB energy expression consists of four terms, including electronic (EL), atom-pairwise repulsion (REP), dispersion (DISP), and halogen-bonding (XB):

$$E_{GFN1-xTB} = E_{EL} + E_{REP} + E_{DISP} + E_{XB} \quad (7)$$

The electronic term is given by:

$$E_{EL} = \sum_{i}^{occ} n_i \langle \psi_i \left| H_0 \right| \psi_i \rangle + \frac{1}{2} \sum_{A,B} \sum_{l(A)} \sum_{l'(B)} p_l^A p_{l'}^B \gamma_{AB,ll'} + \frac{1}{3} \sum_{A} \Gamma_A q_A^3 - T_{el} S_{el} \quad (8)$$

which contains a zeroth-order contribution term $\sum_{i}^{occ} n_i \langle \psi_i \left| H_0 \right| \psi_i \rangle$, a second-order contribution term $\frac{1}{2} \sum_{A,B} \sum_{l(A)} \sum_{l'(B)} p_l^A p_{l'}^B \gamma_{AB,ll'}$, a cubic charge correction term $\frac{1}{3} \sum_{A} \Gamma_A q_A^3$, and an electronic free energy term $T_{el} S_{el}$. In the zeroth-order contribution term, H_0 is the zeroth-order Hamiltonian; ψ_i is the valence molecular orbital indexed by i; and n_i is the occupation number indexed by i. In the second-order contribution term, $\gamma_{AB,ll'}$ is

the semi-empirical electron repulsion operator which depends on the interatomic distance of atoms A and B, as well as further empirical parameters that are specific for different angular momenta l and l'; p_l^A and $p_{l'}^B$ are the monopole charges. In the cubic charge correction term, q_A is the Mulliken charge of atom A; Γ_A is the charge derivative. In the electronic free energy term, T_{el} is the electronic temperature; S_{el} is the electronic entropy. The atom-pairwise repulsion term is given by:

$$E_{REP} = \sum_{AB} \frac{Z_A^{eff} Z_B^{eff}}{R_{AB}} e^{-(\alpha_A \alpha_B)^{1/2} (R_{AB})^{k_f}} \quad (9)$$

where Z_A^{eff} and Z_B^{eff} are effective nuclear charges; k_f is a global parameter; α_A and α_B are element-specific parameters. The dispersion term is computed by the well-established D3 method in the BJ-damping scheme. Self-consistent field (SCF) convergence for the single-point energy calculation was set to be $1E^{-4}$ Hartree.

Electric/ion Field Simulation

The distribution of the electric field and Zn^{2+} concentration field at the anode/electrolyte interface was simulated using a simplified 2D model based on COMSOL Multiphysics software. In this model, the length of two Zn electrodes was 5.0 μm with a thickness of 0.3 μm, as well as an adjacent distance of 3.4 μm. The surface morphologies of bare Zn and PZn electrodes were set based on SEM observations. The voltage hysteresis of the symmetric cells was the same and set as 28 mV at the current density of 1 mA cm^{-2}, where the anodic potential was a constant of 0. The stimulations were performed at the operating temperature of 298 K and an initial ion flux of 2 M in $ZnSO_4$ electrolyte.

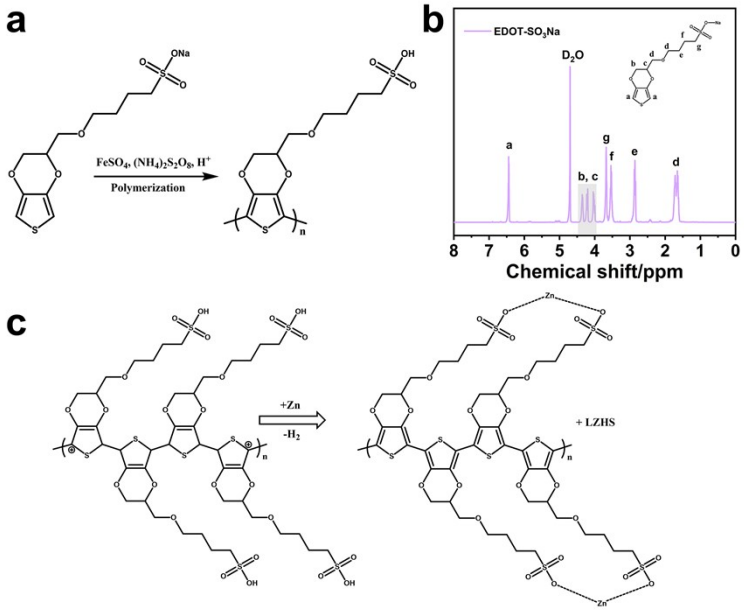

Figure S1. (a) Synthesis route of PEDOT-SO_3H; (b) ^{1}H-NMR of EDOT-SO_3Na monomer; (c) Schematic diagram of the reaction process between polymer solution and Zn foil.

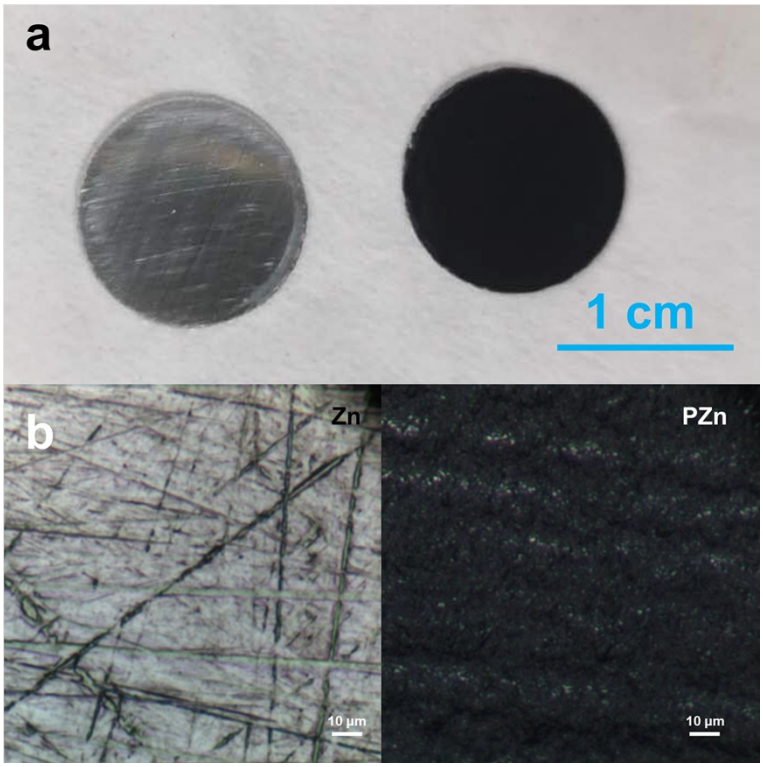

Figure S2. Optical images of Zn foil before/after coating with conducting polymer under different scale bars.

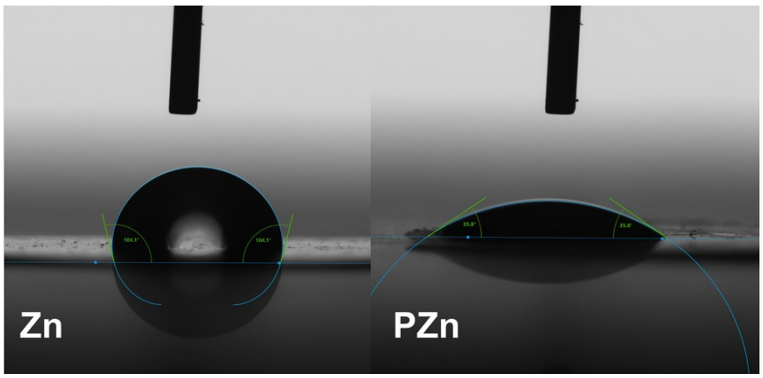

Figure S3. The contact angle of the electrode with the 2 M $ZnSO_4$ electrolyte for bare Zn and PZn.

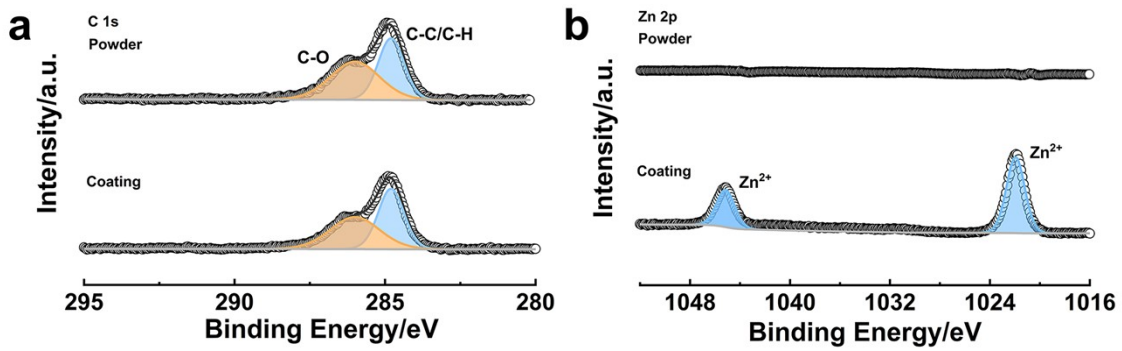

Figure S4. XPS for C 1s (a) and Zn 2p (b) of PEDOT-SH before and after coating on the Zn surface.

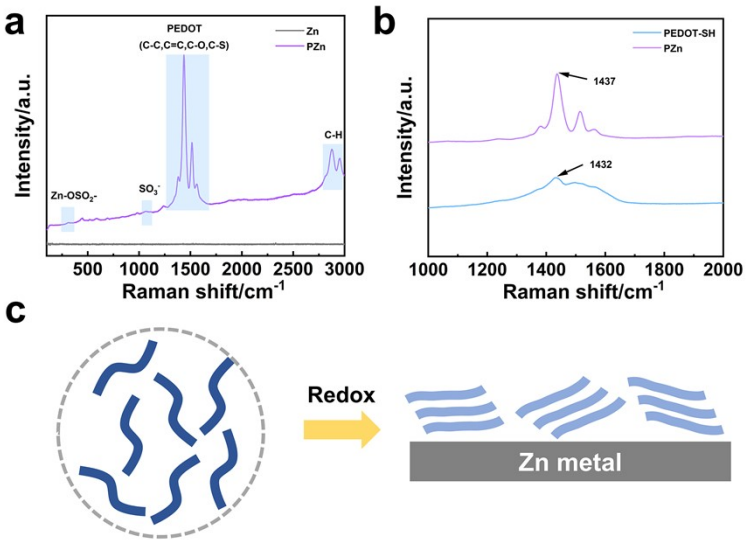

Figure S5. (a) Raman spectra of PEDOT-SH after coating on the Zn surface compared to bare Zn; (b) Raman spectra of the polymer before/after coating on the Zn surface within 1000-2000 cm^{-1}; (c) Schematic diagrams of the configuration/planar regularity changes of the polymer after coating on the Zn surface.

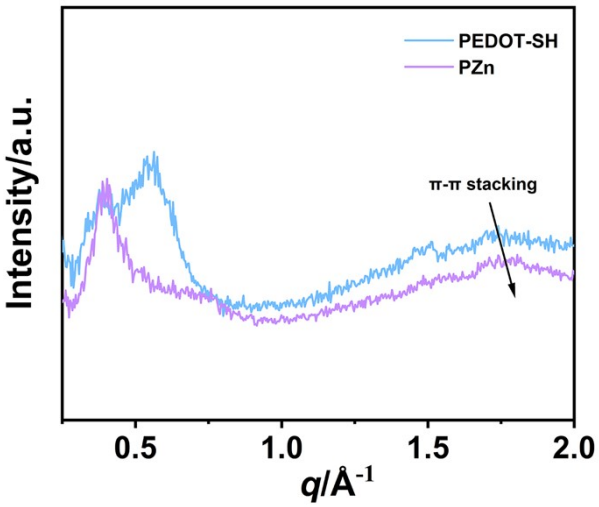

Figure S6. 1D GIWAXS scattering profiles of the PEDOT-SH and PZn after integration.

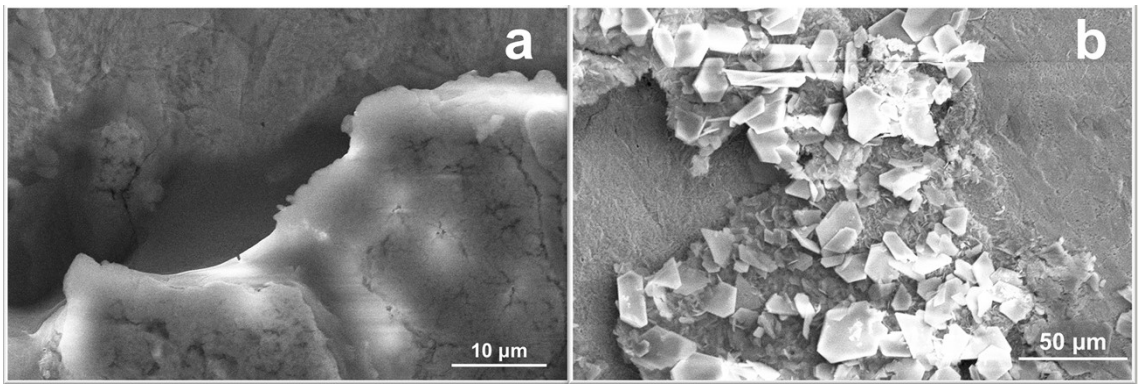

Figure S7. SEM images of bare Zn immersed in H_2SO_4 electrolyte (pH=1) for 1 day (a) and 7 days (b).

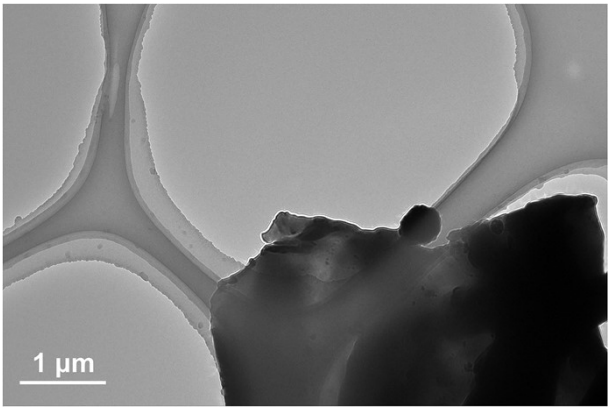

Figure S8. TEM image of the polymer coating dropped on the Cu mesh.

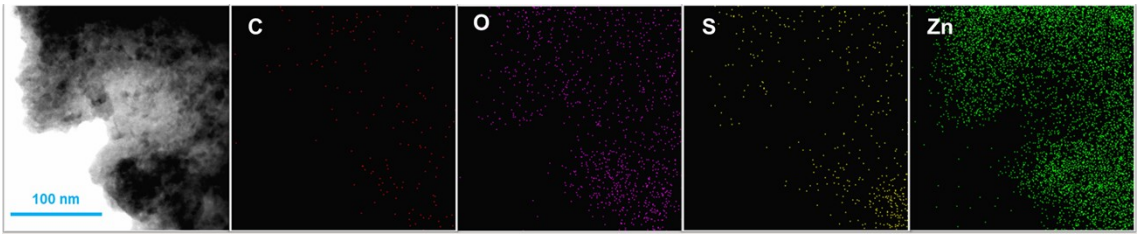

Figure S9. TEM-EDS elemental mapping for polymer coating (C, O, S, and Zn).

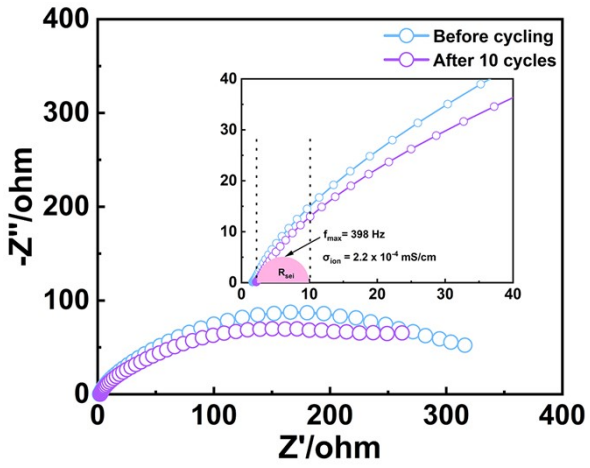

Figure S10. EIS spectra of the pristine PZn//PZn symmetric cell and the cell for 10 cycles at 0.5 mA cm^{-2}, 0.25 mAh cm^{-2}. The inset showed an enlarged image in the dotted boxes of the panel and data fitting curves of impedance.

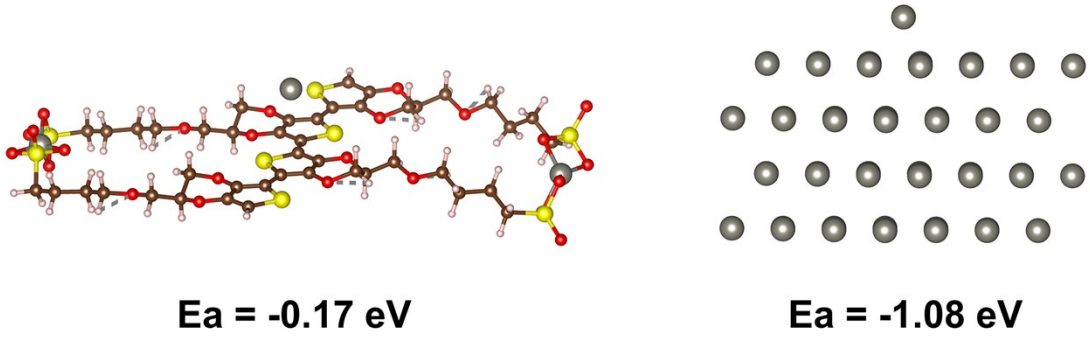

Figure S11. The adsorption energy of the Zn atoms on the conducting polymer and Zn (002) substrates.

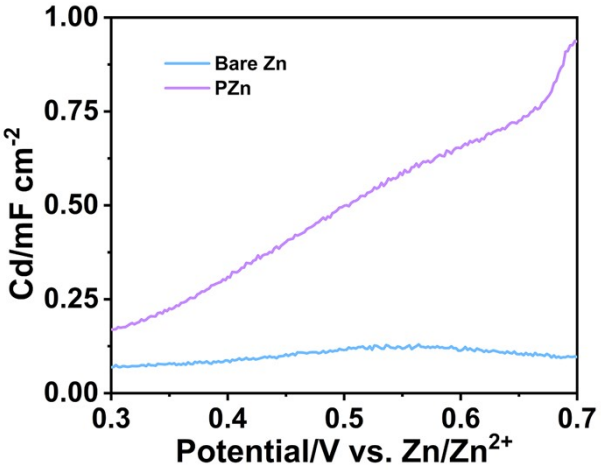

Figure S12. Differential capacitance curves of Cu//Zn cell and PCu//Zn cell using 2 M $ZnSO_4$ electrolyte.

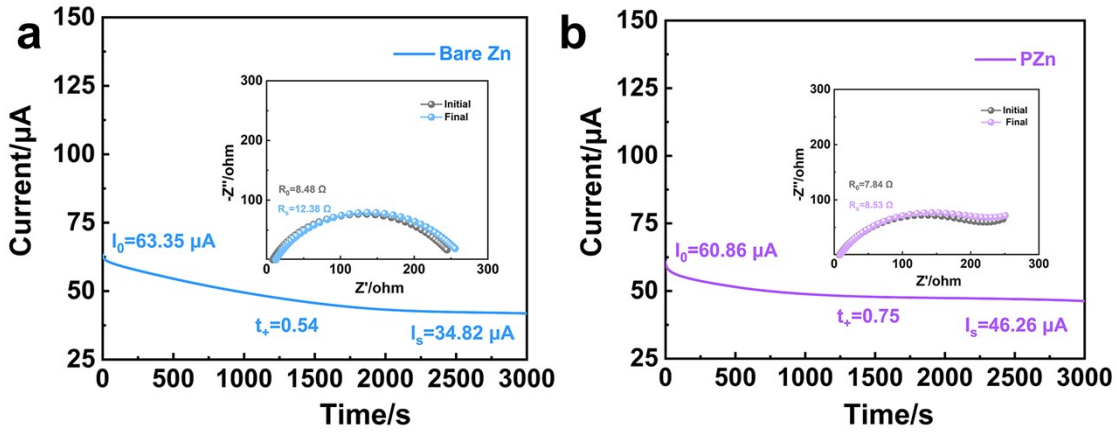

Figure S13. Zn^{2+} transference number of bare Zn (a) and PZn (b) anodes.

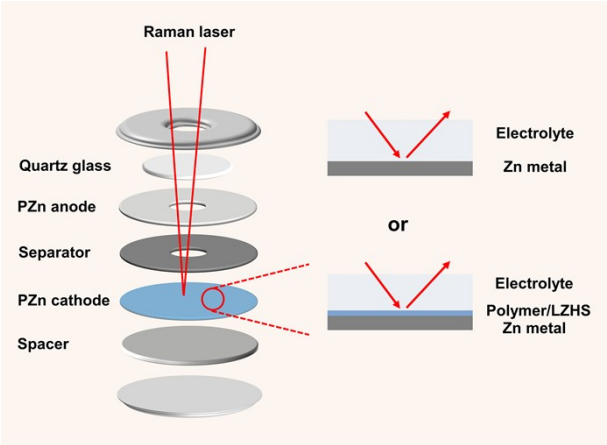

Figure S14. Schematic diagram of the assembled cell for the in-situ Raman test.

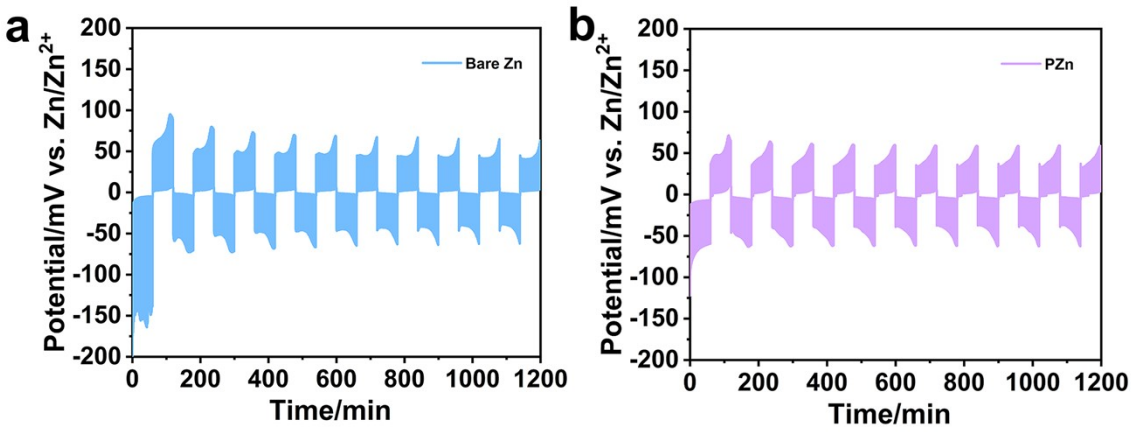

Figure S15. GITT curves of bare Zn//Zn and PZn//PZn symmetric cells operating for 1 min and resting for 1 min at 5 mA cm^{-2}.

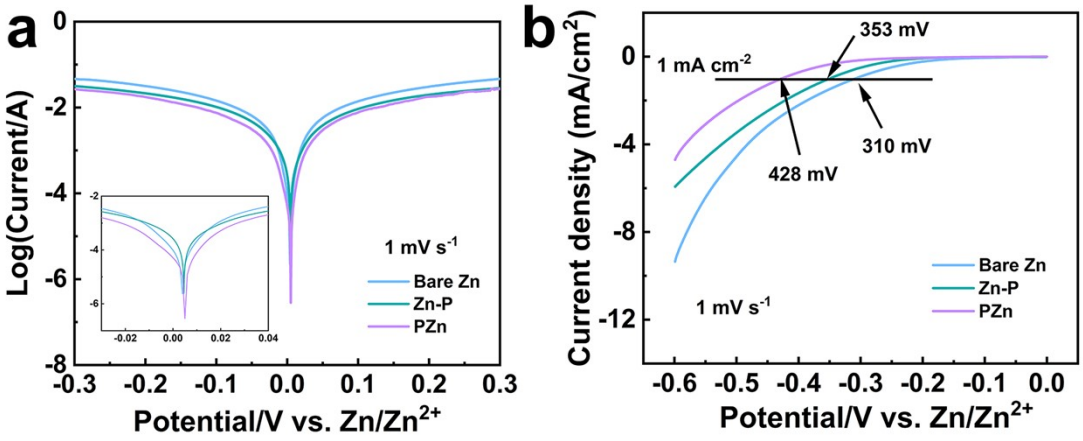

Figure S16. (a) Tafel curves of bare Zn and PZn electrodes; (b) LSV curves of bare Zn and PZn electrodes.

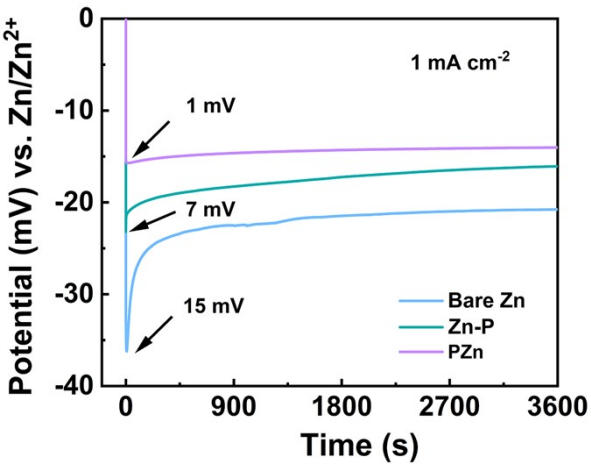

Figure S17. Nucleation overpotentials of Zn deposition under 1 mA cm^{-2} for 3600 s.

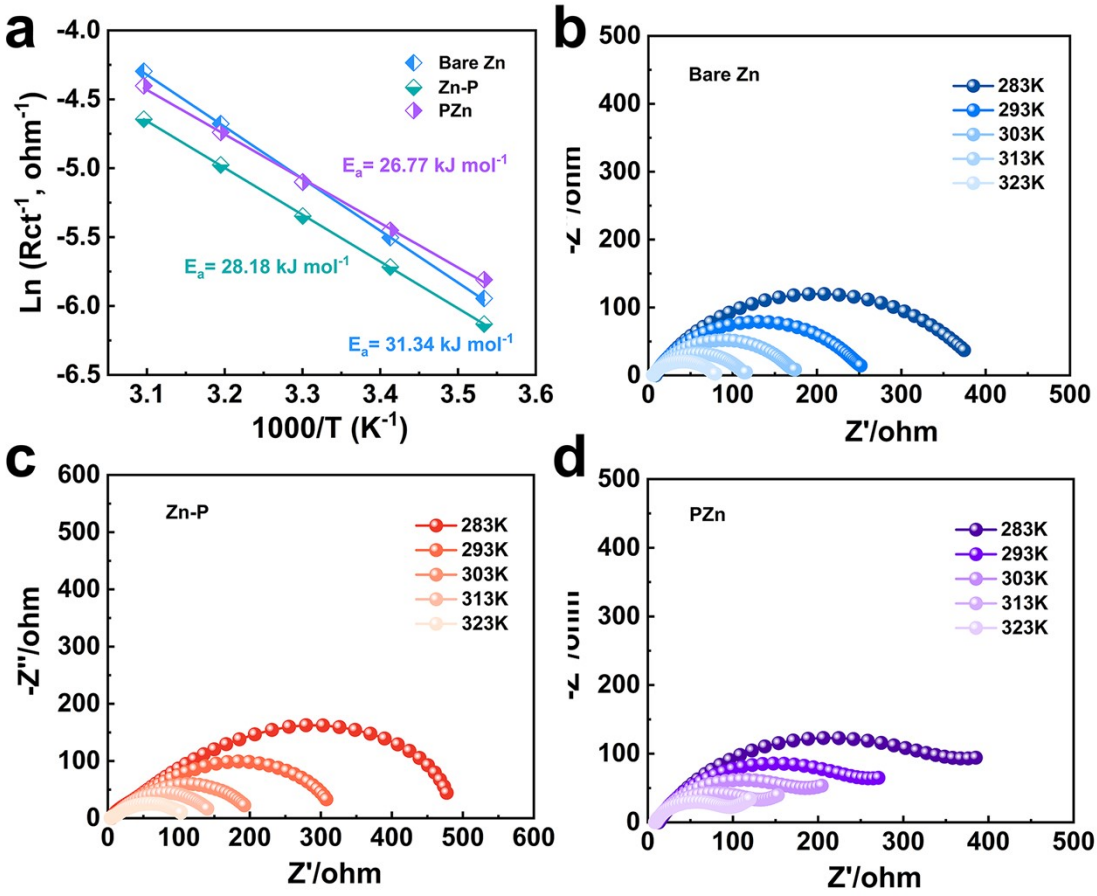

Figure S18. Activation energies (a) calculated from the Arrhenius formula based on the EIS results (b, c) under the different temperatures (283-323 K).

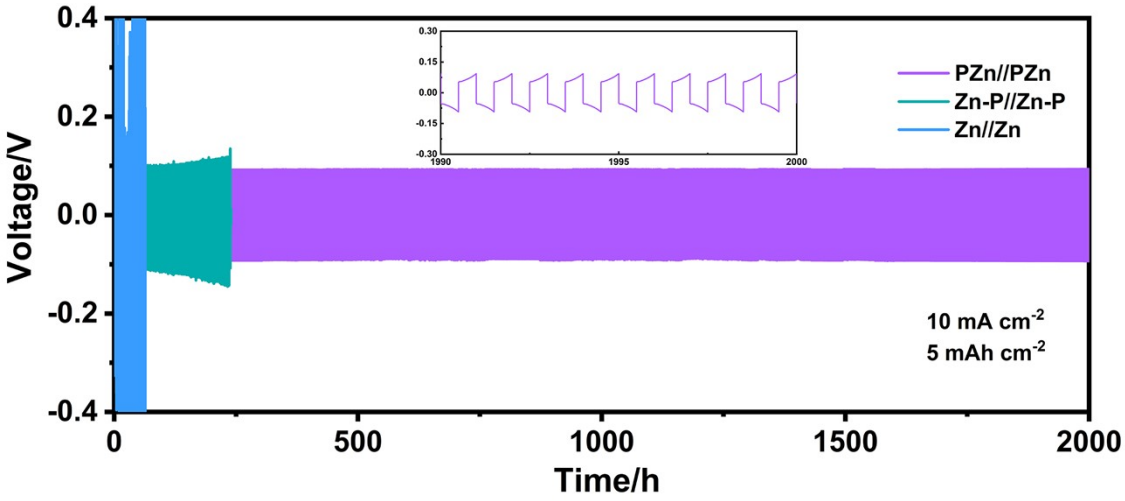

Figure S19. Cycling performances of Zn//Zn symmetric batteries with bare Zn and PZn electrodes at 10 mA cm^{-2}/5 mAh cm^{-2}.

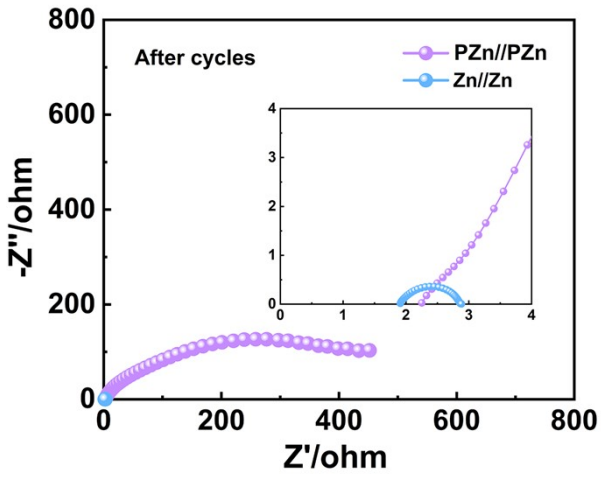

Figure S20. EIS results of the cycled symmetrical cells after cycles at 20 mA cm^{-2}/10 mAh cm^{-2}.

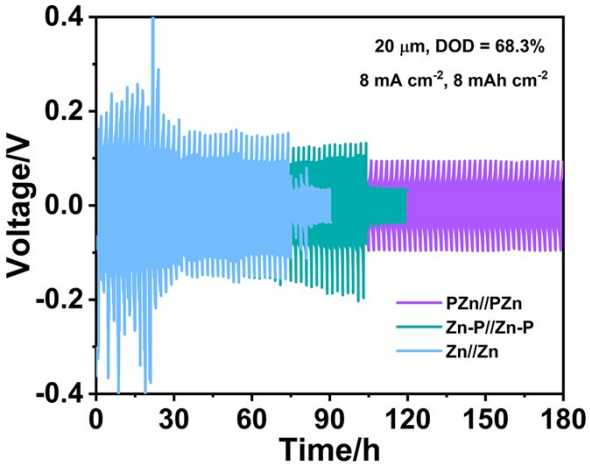

Figure S21. Cycling performance of Zn//Zn symmetric batteries with bare Zn, Zn-P, and PZn at 8 mA cm^{-2}/8 mAh cm^{-2}; DOD: 68.3%.

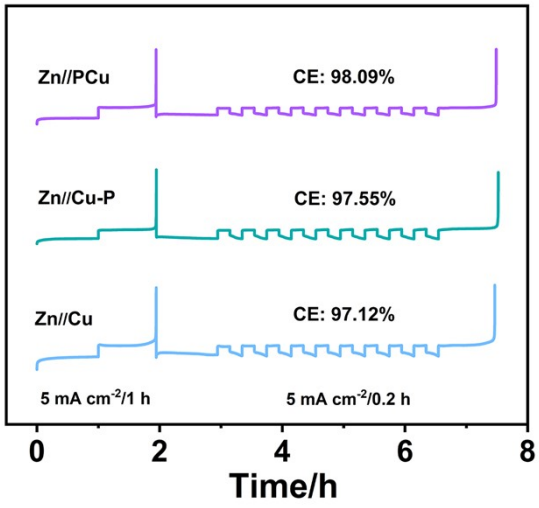

Figure S22. CE of Zn//Cu asymmetric cells at 5 mA cm^{-2}/1 mAh cm^{-2} with a pre-deposition capacity of 5 mAh cm^{-2}.

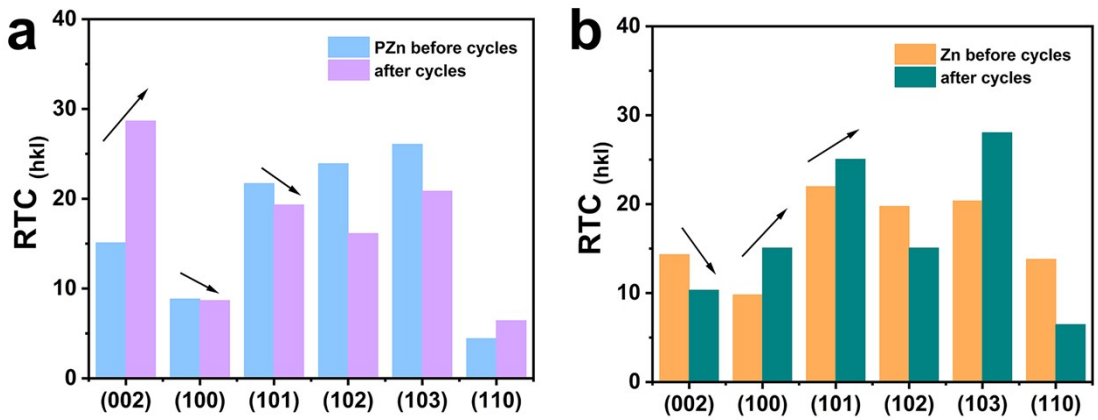

Figure S23. Relative texture coefficients, $RTC_{(hkl)}$ of the Zn (PZn) before/after 100 cycles at 1 mA cm^{-2}/1 mAh cm^{-2}.

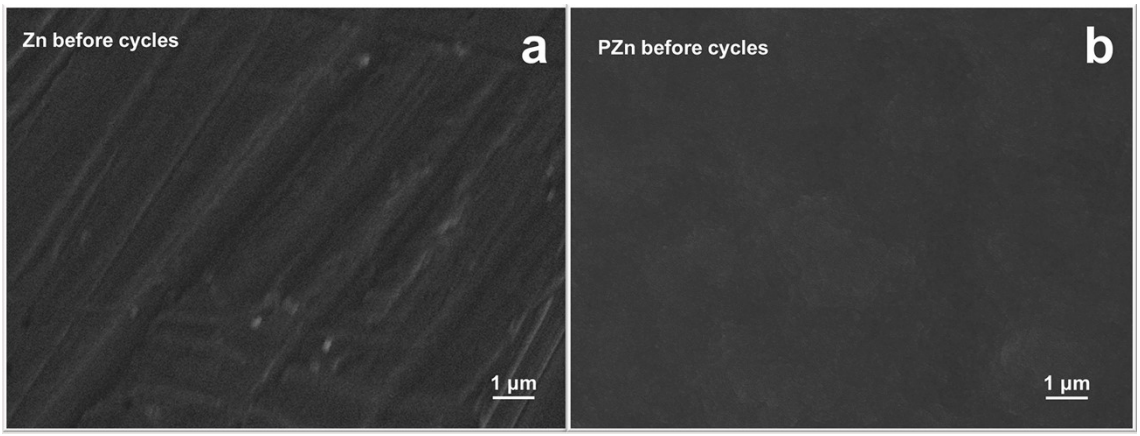

Figure S24. SEM results of the morphology of bare Zn (a) and PZn electrodes (b) before cycles.

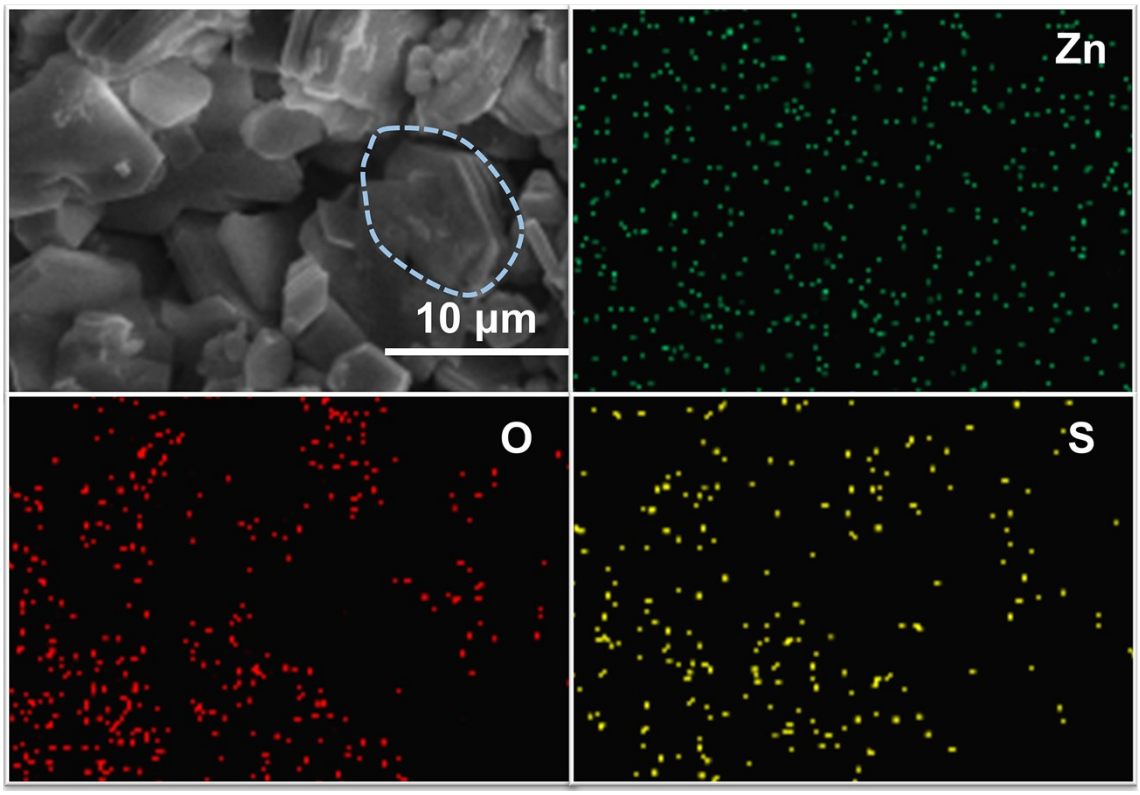

Figure S25. SEM images and corresponding EDS elemental mappings of the cycled PZn electrode.

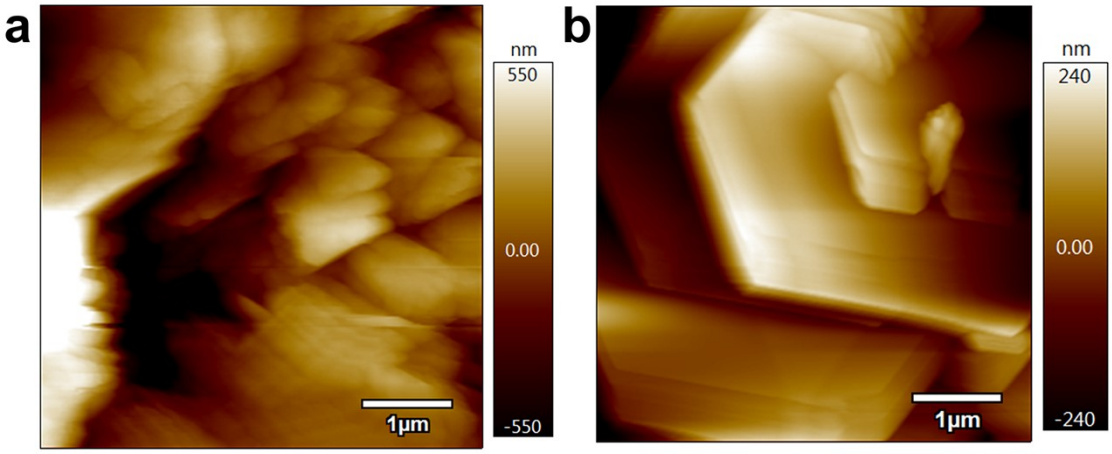

Figure S26. AFM images of bare Zn (a) and PZn (b) electrodes after cycles in a flat.

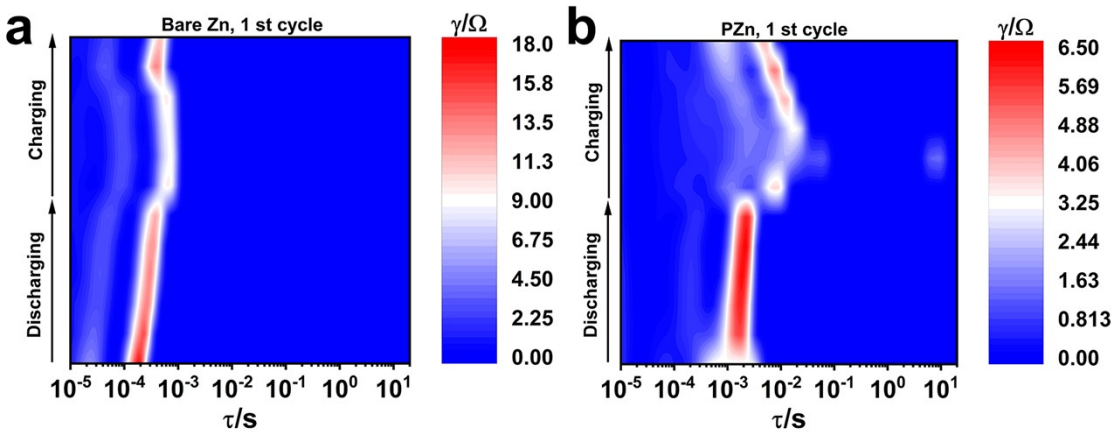

Figure S27. In-situ DRT analysis of plating/stripping process on bare Zn (a) and PZn (b) in symmetric cells (1st cycle).

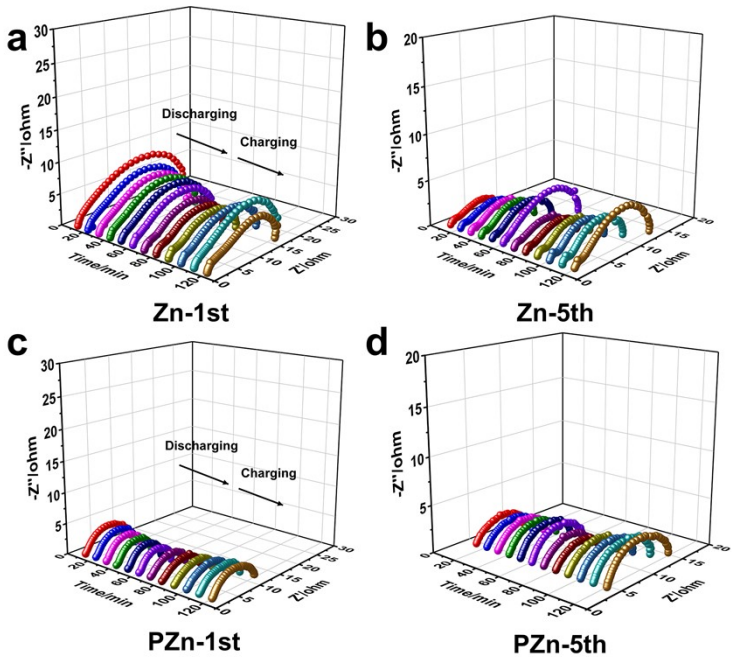

Figure S28. (a, b) In-situ EIS results of the Zn//Zn cells during the discharging/charging process; (c, d) In-situ EIS results of the PZn//PZn cells during the discharging/charging process. EIS data were collected per time after GCD at 1 mA cm^{-2} for 10 min.

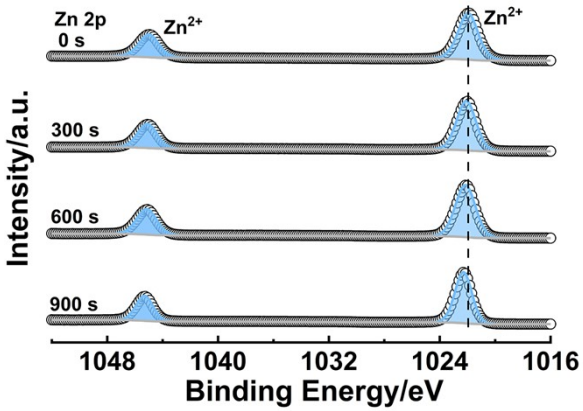

Figure S29. XPS depth profiles for Zn 2p of cycled PZn electrodes.

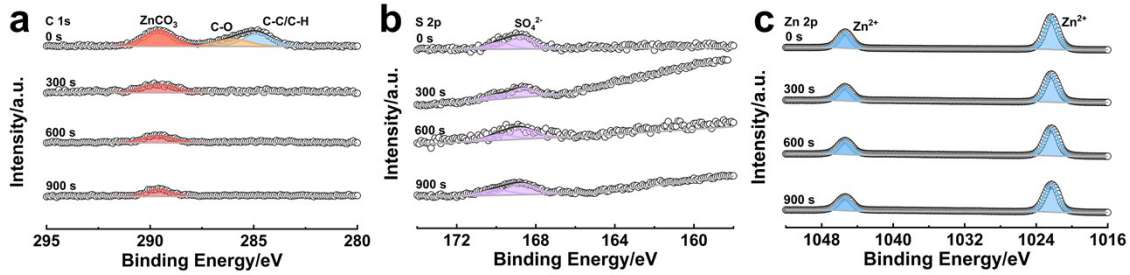

Figure S30. XPS depth profiles for C 1s, S 2p, and Zn 2p of cycled bare Zn electrodes.

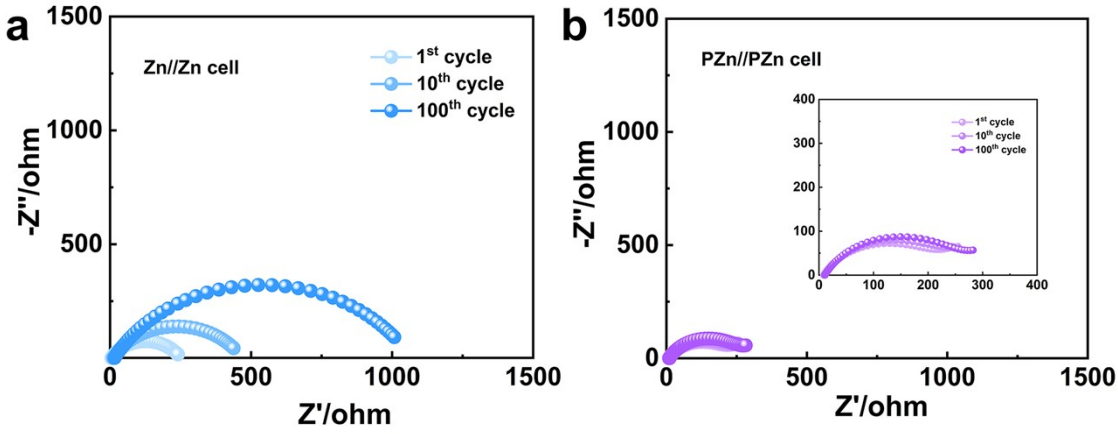

Figure S31. EIS results of Zn//Zn symmetric cells based on the bare Zn (a) and PZn electrodes after different cycles (1, 10, 100 cycles).

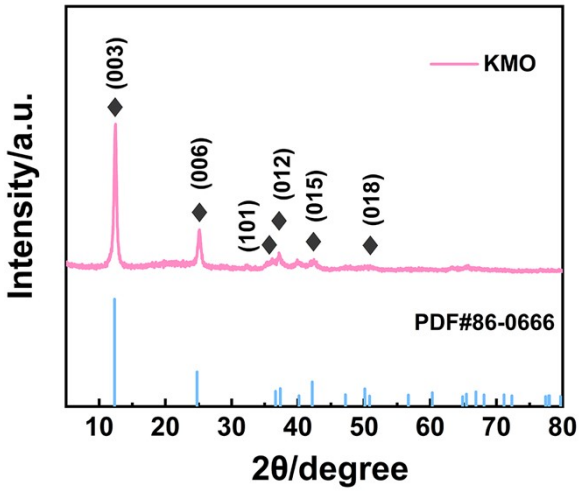

Figure S32. XRD pattern of KMO powder with standard PDF.

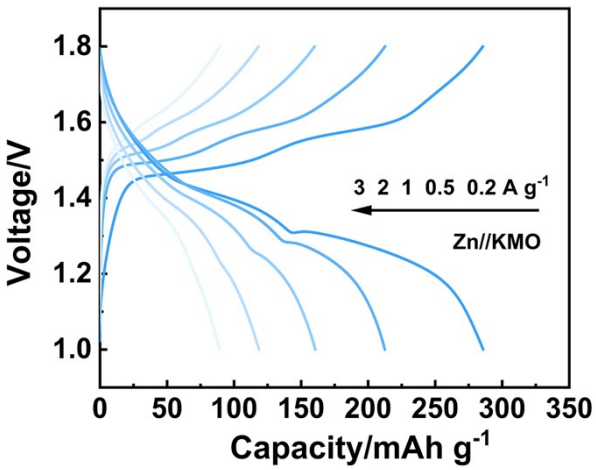

Figure S33. The charging/discharging profiles of the Zn//KMO cells under different current rates.

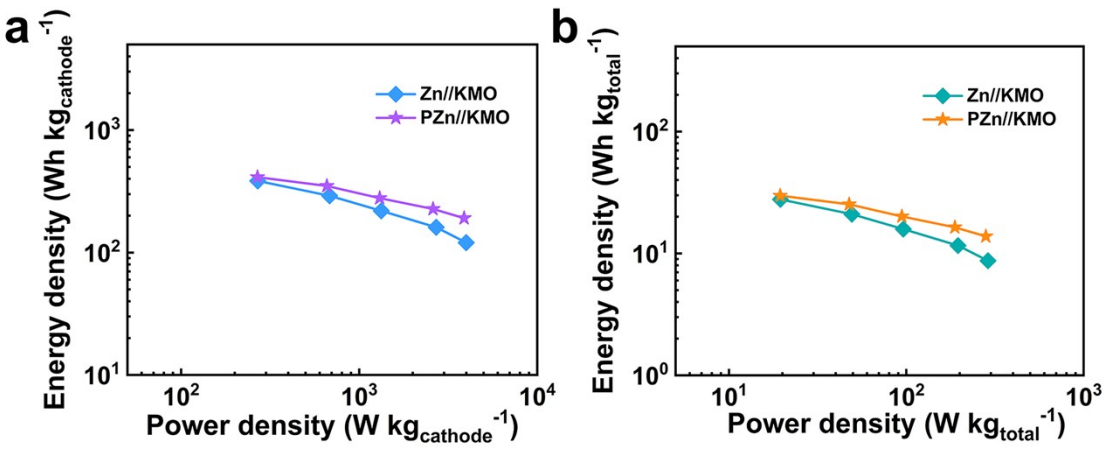

Figure S34. Ragone plots of energy density/powder density based on the mass of KMO (a) and full cell (b). The total mass of the full cell contained the anode, cathode, and electrolyte.

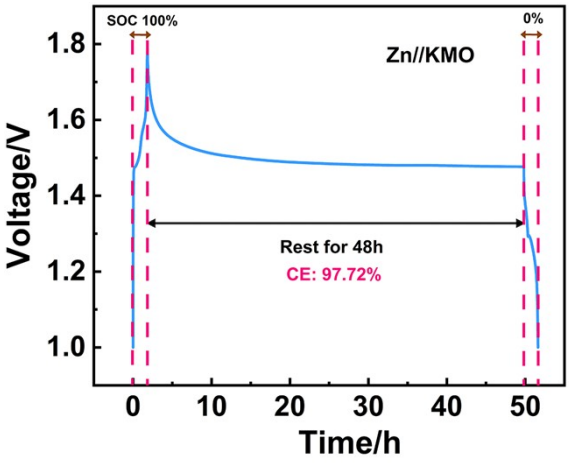

Figure S35. Self-discharge behavior and CE of the Zn//KMO full cell after fully charging and resting for 48 h.

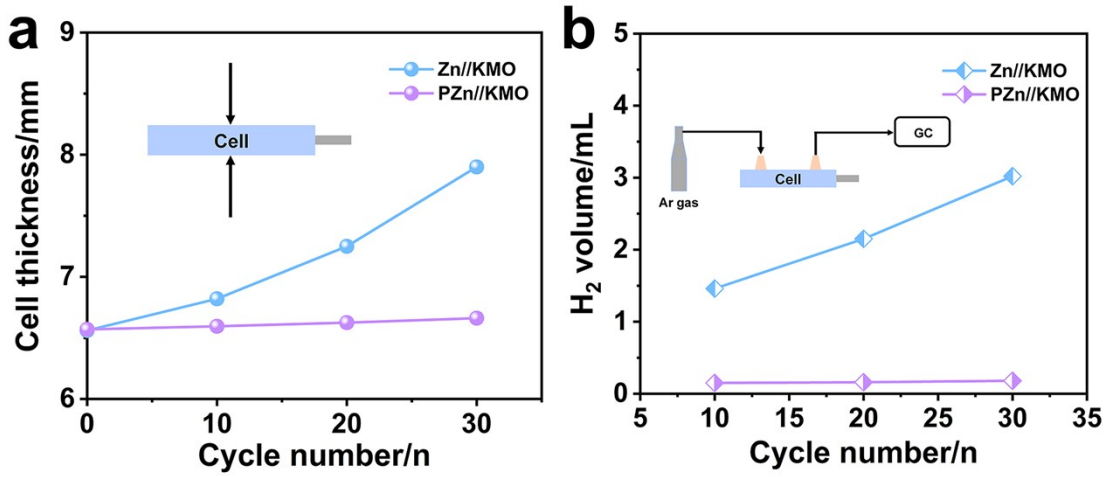

Figure S36. (a) Thickness measurement of the pouch cell after different cycles; (b) Quantization of generated H_2 volume in the pouch cells by GC within first 10 cycles, 10-20 cycles, and 20-30 cycles. Current density: 0.5 A g^{-1}.

Table S1 Performance comparison of the symmetrical Zn//Zn cells with other advanced coated Zn.

Samples	Zn thickness/ μm	Current density/ mA cm^{-2}	Areal capacity/ mAh cm^{-2}	Life time/h	Depth of discharge (DOD)	Ref.
PZn	**100**	**20**	**10**	**200**	**17.1%**	**This work**
	20	**8**	**8**	**100**	**68.3%**	
PEDOT@Zn	50	10	10	780	34.2%	[1]
PgBTTT@Zn	20	2	10	300	85.4%	[2]
PMN@Zn	100	1	20	200	34.2%	[3]
g-C_3N_4/ CP@Zn	100	1	5	3000	8.5%	[4]
FZP@Zn	40	2	14	406	59.8%	[5]
FPI@Zn	10	4	4	500	68.3%	[6]
LZTO@Zn	30	10	10	300	56.9%	[7]
StZ@Zn	100	5	1	4800	1.7%	[8]
MOF-E@Zn	100	5	5	200	8.5%	[9]
FeHCF@Zn	20	2	10	160	85.4%	[10]
MAHEPE@Zn	100	20	4	270	6.8%	[11]
PIM-14@Zn	30	5	5	500	28.5%	[12]
PPAG@Zn	10	2	4	500	68.3%	[13]
FATP@Zn	50	5	5	5000	17.1%	[14]

Table S2 Elements contents on the cycled PZn in SEM-EDS mapping.

Sample	Zn/wt%	O/wt%	S/wt%
Cycled PZn	69.4	24.9	5.7

Reference:

1. D. Wang, N. Zhang, Y. Zhang, L. Chang, H. Tang, W. Zhang and Q. Zhu, Adv. Energy Mater., 2025, **15**, 2404090.
2. H. Zhang, T. Qiu, J. Yang, Y. Ma, C. Ding, L. K. Ono, J. Zeng, W. Liu, S. Zhao, C. Zou, Q. Jiang, Y. Qi, X. Tian and H. Chen, Energy Environ. Sci., 2025, **18**, 5448-5456.
3. D. Luo, B. Niu, P. Du, Q. Lin, L. Hu, Y. Jiang, C. Peng and X. He, Adv. Mater., 2025, **37**, 2418741.
4. H. Li, J. Li, C. Wei, Y. Wang, S. Wang, Y. Chen, G. Bai, K. Zhuo, Z. Bai and J. Lu, Adv. Mater., 2024, **36**, 2410249.
5. J. Li, J. Ba, C. Zhao, F. Duan, X. Yin, Y. Wei, K. Zhao and Y. Wang, Adv. Mater., 2025, **37**, 2501956.
6. Y. Wang, W. Chen, F. Wang, X. Li, Z. Zhang, W. Li and F. Wang, Adv. Mater., 2025, **37**, 2500596.
7. Z. Liu, M. Xi, G. Li, Y. Huang, L. Mao, J. Xu, W. Wang, Z. Qi, J. Ding, S. Zhang and Z. Guo, Adv. Mater., 2025, **37**, 2413677.
8. Y.-F. Qu, J.-W. Qian, F. Zhang, Z. Zhu, Y. Zhu, Z. Hou, Q. Meng, K. Chen, S. X. Dou and L.-F. Chen, Adv. Mater., 2025, **37**, 2413370.
9. R. Zhang, Y. Feng, Y. Ni, B. Zhong, M. Peng, T. Sun, S. Chen, H. Wang, Z. Tao and K. Zhang, Angew. Chem. Int. Ed., 2023, **62**, e202304503.
10. Z. Xu, J. Li, Y. Fu, J. Ba, F. Duan, Y. Wei, C. Wang, K. Zhao and Y. Wang, Energy Environ. Sci., 2025, **18**, 4251-4261.
11. D. Ma, F. Li, K. Ouyang, Q. Chen, J. Zhao, M. Chen, M. Yang, Y. Wang, J. Chen, H. Mi, C. He and P. Zhang, Nat. Commun., 2025, **16**, 4817.
12. Y.-X. Xiao, Z.-Y. Gu, Y. Su, X.-T. Wang, J.-L. Yang, L.-X. Zhang, J.-X. Lin, J.-E. Zheng, Z.-B. Ma, D. Liu and X.-L. Wu, Adv. Funct. Mater., 2026, **36**, e25423.
13. J. Li, C. Wei, M. Zhao, W. Wu, H. Li, R. Hu, G. Bai, K. Zhuo, Z. Bai and J. Lu, Angew. Chem. Int. Ed., 2025, **64**, e202514671.
14. D. Zhang, Y. Chen, X. Zheng, P. Liu, L. Miao, Y. Lv, Z. Song, L. Gan and M. Liu, Angew. Chem. Int. Ed., 2025, **64**, e202500380.